Acta Crystallographica Section B
Structural Science
ISSN 0108-7681

X-ray powder diffraction structure determination of γ-butyrolactone at 180 K: phase-problem solution from the lattice energy minimization with two independent molecules

Robert J. Papoular,[a] Hassan Allouchi,[b] Alexandre Chagnes,[c] A. Dzyabchenko,[d] Bernard Carré,[c] Daniel Lemordant[c] and Viatcheslav Agafonov[c]*

[a]Laboratoire Léon Brillouin, CEA Saclay, F-91191 Gif-sur-Yvette *CEDEX*, France, [b]Laboratoire de Synthèse Physico-Chimique Organique et Thérapeutique (EA 3857), Université de Tours, Facultés des Sciences et Techniques, et de Pharmacie, Parc de Grandmont, 37200 Tours, France, [c] Laboratoire de Chimie-Physique des Interfaces et de Milieux Electrolytiques (EA 2098), Université de Tours, Facultés des Sciences et Techniques, et de Pharmacie, Parc de Grandmont, 37200 Tours, France, and [d]Karpov Institute of Physical Chemistry, 10 Obukha, 103064 Moscow, Russia

Correspondence e-mail: agafonov@univ-tours.fr

Received 20 October 2004
Accepted 17 February 2005

The crystal structure of the solid phase of the dipolar aprotic solvent γ-butyrolactone (BL1), $C_4H_6O_2$, has been solved using the atom–atom potential method and Rietveld-refined against powder diffraction data collected at T = 180 K with a curved position-sensitive detector (INEL CPS120) using Debye–Scherrer diffraction geometry with monochromatic X-rays. It was first deduced from the X-ray experiment that the lattice parameters are a = 10.1282 (4), b = 10.2303 (5), c = 8.3133 (4) Å, β = 93.291 (2)° and that the space group is $P2_1/a$, with Z = 8 and two independent molecules in the asymmetric unit. The structure was then solved by global energy minimization of the crystal-lattice atom–atom potentials. The subsequent *GSAS*-based Rietveld refinement converged to the final crystal-structure model indicator R_{F^2} = 0.0684, profile factors R_p = 0.0517 and R_{wp} = 0.0694, and a reduced χ^2 = 1.671. After further cycles of heating and cooling, a powder diffraction pattern markedly different from the first pattern was obtained, again at T = 180 K, which we tentatively assign to a second polymorph (BL2). All the observed diffraction peaks are well indexed by a triclinic unit cell essentially featuring a doubling of the a axis. An excellent Le Bail fit is obtained, for which R_p = 0.0312 and R_{wp} = 0.0511.

1. Introduction

1.1. Why butyrolactone?

Dipolar aprotic solvents such as lactones, *e.g.* butyrolactone (BL), or alkylcarbonates, *e.g.* propylene carbonate (PC), ethylene carbonate (EC) and other alkylcarbonates, are of great technological importance as components of electrolytes for lithium batteries (Wakihara, 1998; Chagnes, Mialkowski *et al.*, 2001; Mialkowski *et al.*, 2002; Chagnes, Carré, Willmann *et al.*, 2003; Chagnes, Allouchi *et al.*, 2003). γ-Butyrolactone (BL) is an attractive solvent for Li batteries owing to its high boiling point (480 K at 100 kPa), its low melting point (226 K) and its high dielectric constant (39.1 at 298 K; Wakihara, 1998). Nevertheless, it has to be mixed with low viscosity solvents such as dimethylcarbonate (DMC) in order to decrease the viscosity of the solution and enhance the conductivity of the lithium salts added. In addition, the use of a binary mixture of solvents (such as BL-DMC) provides the opportunity to decrease the melting point owing to the formation of a low melting eutectic (Chagnes, Carré, Lemordant & Willmann, 2001; Chagnes, Nicolis *et al.*, 2003).

In a preceding study we investigated the thermodynamic properties of binary liquid mixtures containing BL and DMC (Chagnes, Mialkowski *et al.*, 2001; Chagnes *et al.*, 2002; Chagnes, Nicolis *et al.*, 2003; Lemordant *et al.*, 2002). All excess thermodynamic functions showed that the interaction

between pairs of like molecules is stronger than between pairs of unlike molecules. In particular, we found from the Kirkwood factor value ($g_k < 1$) that intermolecular forces involve an antiparallel alignment of neighbouring dipoles in these mixtures. The structure of BL in the solid state is not known at this time and it will be valuable to determine its structure in order to compare the structure of BL in the liquid and solid states.

1.2. Molecular mechanics and global energy minimization

Molecular mechanics and *ab initio* methods or Monte Carlo simulations are useful tools to calculate the thermodynamic and dynamical properties of liquids, such as transport properties, or to investigate the structure of the solvatation shell around ions. In molecular mechanics methods, a molecule is described as a collection of atoms that interact with each other *via* simple analytical functions called the force field. The accuracy of this computational method depends on the force-field parameters calculated from the experimental data determined by X-ray diffraction experiments. An increasing number of investigations of new force-field parameters have been reported in the literature (Lii, 2002; Allinger *et al.*, 1996; Robinet *et al.*, 2001; Rameau *et al.*, 1998; Andrande *et al.*, 2002; Sun *et al.*, 1994; Allinger *et al.*, 1992). Each force field is evaluated for specific organic functions such as aldehyde or ketone (Allinger *et al.*, 1991), carboxylic acid or ester (Allinger *et al.*, 1991), carbonate (Sun *et al.*, 1995; Soetens *et al.*, 2001; Allen & Tildesley, 1987; Matias *et al.*, 1989; Dauber-Osguthorpe *et al.*, 1981) or lactone.

In recent years, a number of crystal structures of organic molecular compounds have been determined by X-ray powder diffraction from data collected using conventional X-ray sources. Most of these structures were determined at room temperature using well prepared powders but, in our opinion, few structures of organic compounds were determined at low temperatures. In this paper, the crystal structure of BL, which is a liquid at room temperature, was determined at 180 K using the atom–atom potential method. These data may be very useful to understand the structure of this solvent in the liquid state.

Crystal structure modeling based on lattice energy minimization with semi-empirical atom–atom potential functions has long been proven to be useful in the single-crystal structure determination of small organic molecules, in particular whenever the direct methods of structure solution failed because of insufficient quality or quantity (lack of higher θ-range information) of diffraction data. Nowadays, there is a renewed interest in this technique in connection with progress in experimental powder diffraction methods towards full structure determination of polycrystalline materials (Louër *et al.*, 1995; Karfunkel *et al.*, 1996). Moreover, even if the powder pattern is insufficient for structure refinement (for instance, because of severe texturing), but still can be indexed, the experimental cell parameters may provide key information on the selection of the structural model out of the list of low-energy structures generated theoretically. Thus, the polymorphic phenomena studied *in situ* by powder diffraction may demonstrate unstable transient states, whose powder spectra intensities are not suitable for structure determination because of experimental limitations. At the same time the 2θ positions of the diffraction lines are not perturbed by texture and they may therefore be used to decrease the number of potential acceptable theoretical structures.

Before discussing the details involved in our present study, the reader is referred to our previous work (Dzyabchenko & Agafonov, 1995) for a simple outline of our solution approach by means of Global Energy Minimization (GEM) and Packing of Molecules in Crystal analysis (PMC).

1.3. Computation complexity and its reduction using symmetry considerations

In this work we face the problem of a crystal structure solution containing two independent molecules. There are known examples in the relevant literature of the *ab initio* phase problem solution for structures with two independent organic molecules (see, for example, Rukiah, Lefebvre, Hemon & Dzyabchenko, 2004; Rukiah, Lefebvre, Hernandez *et al.*, 2004). Nevertheless, we are particularly interested in the use of global energy minimization as an instrument for structure solution when reliable diffraction data are limited (or even fully absent!). As in the case of an intensity-based search, the presence of a second independent molecule increases the number of trial structures in the 12-dimensional parameter space enormously, provided that neither molecule is constrained *via* a special position. As a matter of fact, in the case of one molecule, one may use the equivalences that exist due to the alternative choices of the crystal axes and the origin permitted by the given space group (Hirshfeld, 1968; Dzyabchenko, 1983) to greatly restrict the asymmetric part of the rigid-body parameter space. Thus, with the present structure, the grid of translational parameters may be restricted to a box of $a/2 * b/2 * c/2$, while the range of one Euler angle (out of three) may be reduced by a factor of two. With each translational parameter allowed to take only two values (say, 1/8 and 3/8) in the range [0,1/2], and a 30° increment for each Euler angle (say, 15, 45° *etc.*), our procedure results in a six-dimensional grid of $8 \times 12 \times 6 \times 6 = 3456$ trial structures, whose minimization can be carried out within a few hours on a regular desktop PC machine. However, with two independent molecules the ranges of the six parameters of the second molecule cannot be confined so radically as those of the first one, since the choice of the crystal axes and origin has already been made. Rather, the equivalences due to the space group are still valid and thus allow us to divide the number of trial structures by the number of equivalent positions. Last, one more reduction of the grid points by a factor of two comes from the fact that the two molecules are identical and their permutations do not violate the crystal configuration. Altogether, the multiplication of the 3456 parameter sets of the first molecule by the $64 \times 12 \times 6 \times 12/(4 \times 2) = 6912$ parameter sets of the second molecule results in a total number of trial structures amounting to some 24 million. At this point, we

note that the use of an idealized (planar) molecular symmetry further enables us to reduce the grid ranges (Hirshfeld, 1968; Dzyabchenko, 1983). Thus, on neglecting the nonplanarity of the lactone ring, the present molecule turns out to have an approximate mirror symmetry, which allows the reduction of the number of unique grid points further down to 6 million.

Previous structure prediction work involves the systematic search of benzene structures within the framework of the $P2_1/c$ space group, $Z = 4$, with two independent molecules at inequivalent symmetry centres (Dzyabchenko, 1987). The systematic grid search was applied for the prediction of biphenyl structures (Dzyabchenko & Scheraga, 2004). van Eijck & Kroon (2000*a*,*b*) and van Eijck (2002) applied a random search method in the structure prediction study of hexapyranoses and polyalcohols of flexible geometry with several independent molecules. Pillardy *et al.* (2001) suggested a Monte-Carlo based procedure for a structure search without symmetry constraints and tested it for a number of organic molecules with conformational degrees of freedom. Therefore, it seems promising to introduce global energy minimization algorithms into the practice of structure determinations of regular organic crystals lacking experimental diffraction data. To the best of our knowledge, the energy-based powder structure determinations published in this latter way has not involved structures with more than one independent molecule per unit cell.

1.4. Improved global energy mimization algorithm using the method of valleys

In this paper we describe the application of a new procedure of global energy minimization, whose principal idea is based on the method of valleys (Gel'fand & Tsetlin, 1962), for the solution of the crystal structure of the γ-butyrolactone polymorph BL1. The method of valleys was routinely used in early X-ray structure determinations of simple organic molecules (Gel'fand *et al.*, 1966) by the global minimization of the *R* factor calculated on single-crystal diffraction data. The basic assumption of the valley method is that the potential function $F(\mathbf{x})$ is properly organized, *i.e.* there are directions in the $\mathbf{x}$ space where this function falls down rapidly and there are ones along which it changes slowly. A simple procedure to organize walking over the valleys is to build the $(i + 1)$th starting point for the minimization in the direction of the line passing through the minimized points $\mathbf{x}_i$ and $\mathbf{x}_{i-1}$ found in the two preceding steps, at some distance λ from $\mathbf{x}_i$, which is a parameter of the method. The second basic parameter is a function threshold Δ, which represents the minimal reduction in F upon which local minimization is terminated. The key feature is that Δ should not be too small to prevent collapsing of the two subsequent minimized points into a single minimum resulting in the principal path direction being lost. Thus, with a suitable choice of λ and Δ, the path $\{\mathbf{x}_i\}$ of the minimized points is believed to develop close to the actual bed of the valley while, at the same time, not locking into some limited region of parameter space but rather being capable of penetrating adjacent valleys over low-height potential barriers (Gel'fand *et al.*, 1966).

2. Experimental

The solvent BL (99.9%) was purchased by Aldrich. X-ray measurements were carried out with an INEL CPS 120 detector using monochromatic Cu $K\alpha_1$ radiation (λ = 1.54056 Å). The alignment of the diffractometer was checked with standard reference materials (Louër, 1991). The angular zero offset error was measured to be less than 0.01° (2θ). The instrumental resolution function (IRF) has been described by Louër & Langford (1988). The precise determination of peak positions was carried out with *FullProf*2k (Rodriguez-Carvajal, 2004) using the *WinPloTR* package (Roisnel & Rodriguez-Carvajal, 2002).

The BL sample was introduced into a 0.5 mm diameter Lindemann glass capillary that was sealed to ensure that no hydration phenomenon occurs during XRD investigations at low temperature. The sample was mounted at the center of the goniometer and was rotated around the θ axis to ensure suitable averaging over crystallites.

The sample was then cooled down to 100 K at 6 K min^{-1} using nitrogen gas vaporized from the liquid in a cryogenic tank (Oxford System Cryosystems 700) in order to obtain a solid phase for XRD investigations. The sample was heated step by step up to 180 K and the XRD patterns were recorded every 10 K. All patterns were found to be perfectly identical and confirm that no phase transition occurs within this range of temperature. In order to investigate the structure of BL, an XRD pattern was accumulated at 180 K over 18 h (BL1). Thereafter, the sample was heated up to 230 K (up to the fusion of the sample) and cooled (quenched) down again to 100 K. The XRD patterns (about 13 patterns) obtained under these conditions from 100 to 230 K (up to fusion) were different from those obtained previously. We believe that a new polymorphic phase has appeared (quoted as BL2 hereafter). No transition between the two phases BL1 and BL2 was found. Additional experiments demonstrate that upon subsequent heating/quenching above the melting point (*ca* 230 K), the newly found polymorph BL2 reverts to its BL1 counterpart.

3. Preliminary data analysis and indexing

3.1. BL1 polymorph

Indexing of the powder diffraction pattern of BL (BL1 phase) was performed using the X-ray data collected using the collected successive dichotomy method (Louër & Louër, 1972), using the PC version of the program *DICVOL*91 (Boultif & Louër, 1991). Our data extend up to above 2θ = 114°, but were trimmed down to $2\theta = 40°$ since no appreciable Bragg peaks could be found above 40°. The corresponding spatial D resolution is 2.252 Å at $2\theta = 40°$ for Cu $K\alpha_1$ radiation. The first 30 diffraction lines were completely indexed on the basis of a monoclinic unit cell. Refinement of the cell

dimensions from the complete powder diffraction data yielded a = 10.1282 (4), b = 10.2303 (5), c = 8.3133 (4) Å, β = 93.291 (2)°, V = 859.95 (7) Å^3. A possible space group was $P2_1/a$ (No.14), for which the final figures of merit were M_{22} = 22, M'_{22} = 66.1, F_{22} = 40.2. Assuming a volume of 18 Å^3 per non-H atom leads to eight $C_4H_6O_2$ molecular units in the unit cell and consequently suggests the presence of two unique ones in the asymmetric unit since the space-group multiplicity can be no larger than 4.

3.2. BL2 polymorph

The powder pattern of the second phase (BL2) has been indexed as triclinic with a = 20.268 (1), b = 10.237 (1), c = 8.320 (1) Å, α = 89.94 (1), β = 93.24 (1), γ = 90.18 (1)°. All the observed diffraction lines are properly accounted for by this cell, which is twice the size of the BL1 cell (note the doubling along the a axis). All our attempts to use *DICVOL*91 in order to find a satisfactory unit cell failed and so did our attempts to use the other widespread *WinPlotR*-based indexing programs, *TREOR* and *ITO*. An alternative successful strategy will be reported elsewhere (Agafonov *et al.*, to be published). An excellent Le Bail fit was obtained over the whole 2θ range (7–69°) over which sizable Bragg peaks could be observed, yielding R_p = 0.0312, R_{wp} = 0.0511 and a Durbin–Watson d-statistics indicator of 1.176. Figs. 1(*a*) and (*b*) display the significantly different diffraction patterns observed for the two polymorphs over the same (10–40°) 2θ range. The full information can be retrieved from the CIF files deposited with this paper (Rietveld fit for BL1, Le Bail fit for BL2). The most delicate part of this analysis is linked to the few weak extra lines that show up with the BL2 polymorph. Our assumption that the latter do in fact belong to the BL2 phase rather than to some impurity phase is further based on some newer complementary measurements we have carried out using monochromatic Co $K\alpha_1$ radiation and some freshly prepared new BL sample at the same temperature (180 K). It is then indeed observed that the same weak extra peaks show up with the BL2 polymorph and then disappear when the latter reverts to its BL1 counterpart after further heating/quenching thermal treatment.

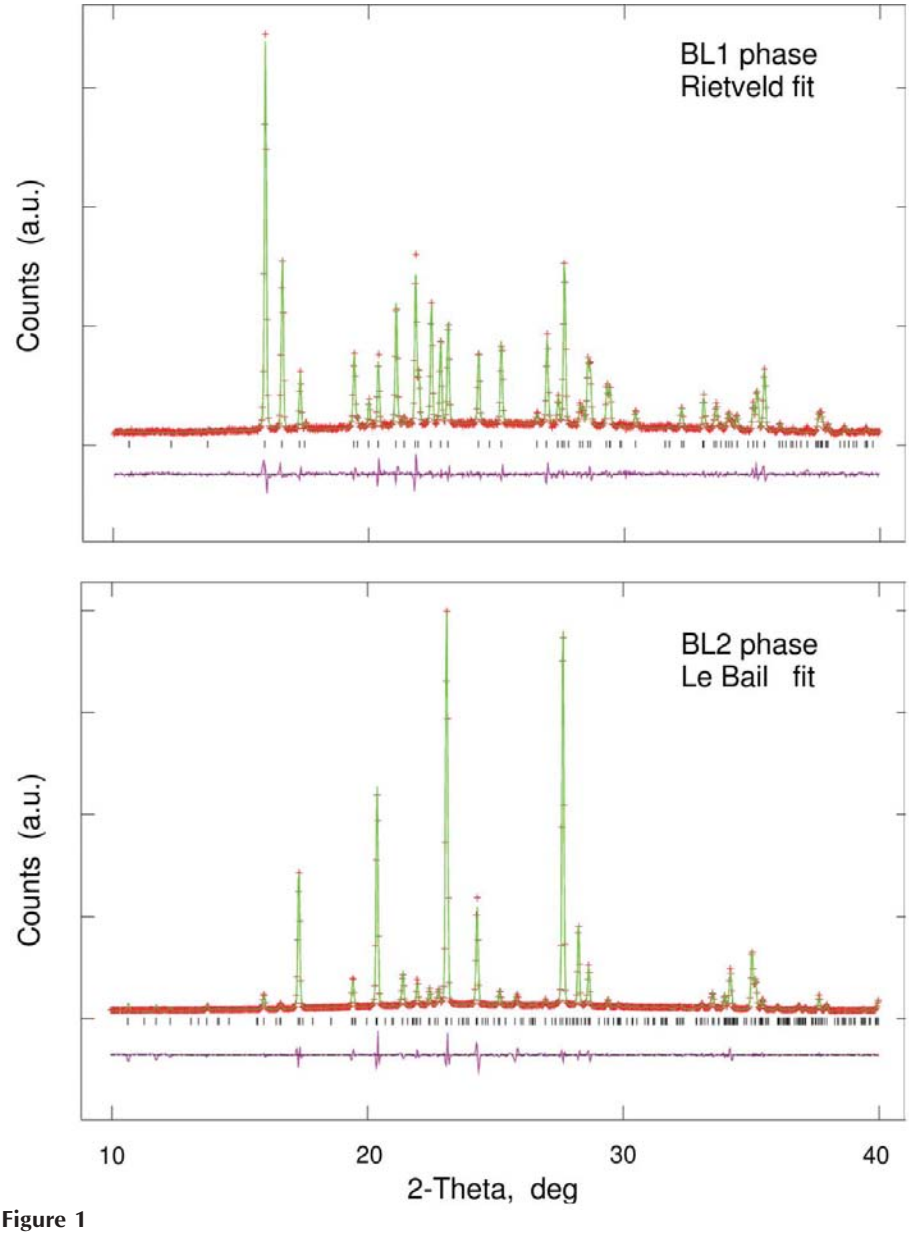

Figure 1
Calculated and experimental XRD spectra of BL at T = 180 K. (*a*) Rietveld fit for BL1 polymorph; (*b*) Le Bail fit for BL2 polymorph.

4. Structure solution and structure refinement

4.1. Structure solution

4.1.1. Molecular model and lattice energy parameters. The molecular model for the packing calculations was obtained by optimization of the lactone geometry with the B3LYP/6-31G method on *GAUSSIAN*98 (Frisch *et al.*, 1998). The optimized lactone conformation was found to be almost planar for all the non-H atoms except C2, which was substantially out of the average plane (see §5). The lattice energy was calculated with the Lennard–Jones 6–12 atom–atom potentials of Momany (Momany *et al.*, 1974) for the van der Waals energy. The Coulomb energy terms were

Table 1
Variation of quality factors with preferred orientation order (spherical harmonics).

PO order	No. of terms, Sph_H	Texture index	Reduced χ^2	$R(F^2)$	R_{wp}	R_p	Durbin–Watson	Redundancy factor
10	35	4.571	1.669	0.0667	0.0694	0.0517	1.180	1.421
8	24	2.326	1.735	0.0879	0.0710	0.0532	1.146	1.761
6	15	1.600	2.326	0.1538	0.0822	0.0619	0.913	2.189
4	8	1.459	3.380	0.2217	0.0991	0.0714	0.686	2.700
2	3	1.039	5.107	0.2847	0.1237	0.0857	0.509	3.240
0	0	1.000	5.542	0.2511	0.1294	0.0894	0.478	3.682

calculated with the atomic net charges obtained with Gasteiger's method (Gasteiger & Marsili, 1980): 0.4 and −0.4 on the C and O atoms of the carbonyl group, −0.17 on the ring oxygen, 0.13 on the aliphatic carbon closest to the ring oxygen and 0.04 e on the cycle carbon closest to the carbonyl; the other two C atoms and all the H atoms had zero charges.

4.1.2. Valley search of low-energy structures using the *PMC* program. The low-energy structures were sought using a version of the *PMC* (Packing of Molecules in Crystals) program (Dzyabchenko, 2001) modified to incorporate the new search routine VALLEY, the basic idea of which is discussed in §1. In a preliminary step, many trial runs of this procedure were performed to obtain the suitable parameters λ and Δ. The objective was to achieve a generation of valley paths with a large number of successive x_i points that would essentially sample the global parameter space at a low height above the energy minima. We were not, however, successful with the λ constant; such a constant parameter could not work universally in the very different energy landscapes that occur in the course of different steps. Progress was made with a value of λ adapted for each step under some restricting conditions. Thus, we required that the shift vector have at least one component greater than 0.1 as an absolute value for a translation parameter (measured as a fraction of the respective unit-cell length) or 15° for an Euler angle. If the minimized point x_{i+1} was closer to x_i than this criterion, the $i + 1$ step was attempted once again with an increased value of λ. On the upper limit, the condition on λ was that the resulting net translation of any of the two molecules be less than 1.5 Å with the net rotation being within 45°. Furthermore, if a minimized point occurred at a very high energy level (> 4000 J mol^{-1}), the step was retried with a reduced value of λ. The parameter Δ = 1 kJ mol^{-1} was found to be satisfactory for the present work. The procedure was not stable enough to generate successful paths of infinite length since in some instances it failed to produce a step to another energy basin. In such a case it was terminated automatically for starting another path. The same course of action was taken with paths found to be oscillating between two or more energy basins, or paths which were cyclically closed. In our computer experiments the path lengths varied from a few steps to 1000 steps.

While searching the structure solution with the VALLEY routine a few dozen paths were generated from points selected at random from a grid in the 12-dimensional parameter space, having an increment of $\frac{1}{4}$ for each translation parameter and an increment of 30° for each Euler angle. The unit-cell parameters were fixed at their X-ray experimentally determined values. The valley-path points were further optimized until full convergence to their respective energy minima. These minima were ranked by energy. As the next step, the lowest-energy structures were tested and ranked according to their related *R* factors calculated using the XRFACT procedure of the *PMC* program. One structure, ranked seventh (which turns out to be ninth after subsequent test calculations which revealed two more minima), produced a low *R* factor of ∼ 30% (featuring 97 peak amplitudes with $2\theta < 45°$), which dropped to 20% after the refinement of this structure with the 12 rigid-body parameters.

4.1.3. Comparison of the valley method with other global energy minimization procedures. To obtain an idea of how efficient the valley method is in comparison with other global minimization methods, we ran the procedure from various grid points. A total of 935 paths containing 67 678 path points have been generated. Their final minimization resulted in 2500 minima within the energy window of 5 kJ mol^{-1} above the global minimum, 22 hits of the global minimum itself and 23 hits of the true structure minimum (all counts include the hits of equivalent minima but disregard the hits of the same minimum from connected same-path points). The average computing time for the generation of each 10^4 path points with their final minimization was 25 h (on a desktop PC equipped with a 2 GHz AMD processor).

For comparison, direct minimizations starting from 30 000 points, which were selected randomly from the 6 million grid points, have succeeded in reaching the true structure minimum only twice. The global minimum in this random search occurred eight times, while a total of 756 non-unique minima were within the energy window of 5 kJ mol^{-1}. The computing time per 10^4 minimizations was 21 h, insignificantly less than in the case of the valley search. Along these lines and in the context of our lactone structure, the valley method demonstrated a far better efficiency with regard to the location of the true structure minimum than the random search (7.5 h *versus* 31.5 h per hit).

4.2. Structure refinement

4.2.1. Le Bail refinement. The atomic coordinates of the rigid-body model obtained from *PMC* were entered into the Le Bail/Rietveld refinement program suite *GSAS* for *Windows* (Larson & Von Dreele, 1987) using the data set collected with the PSD limited to the nominal range 10–40° (2θ). First, 19 fixed data points were selected using *WinPlotR* and a linear interpolation was used to obtain the preliminary background contribution. A Le Bail refinement pass was then run to determine the following nine parameters in the

following order: 2θ offset, LX, GW, LATT (a, b, c, β), GU and GV, where LX, GU, GV and GW pertain to the broadening of the Bragg linewidth *versus* 2θ. The following quality factors were obtained: $\chi^2 = 1.34$, $wR_p = 0.0698$, $R_p = 0.0520$, Durbin–Watson d-statistics = 1.181. There were 81 indexed unique peaks found in the above-mentioned 2θ range and these were used in the subsequent Rietveld structural refinement. No extra peak was left unaccounted for. Finally, it is worth mentioning that a slightly wider 2θ range (10–42.155°) featuring 93 Bragg reflections was used to properly account for the 81 intensities of interest. This is due to our chosen criterion as to how far a given Bragg peak extends (0.01% of its maximum). Relaxing this criterion down to 10% yields an effective 2θ range that contains only the 81 reflections of interest, but results in poorer fits.

4.2.2. Setting up restraints. Prior to actually carrying out the Rietveld structural refinement, one must notice that the total number of structural parameters is huge (with respect to the 81 peaks) and of the order of $3 \times 2 \times 12 + 1 = 73$, including only positional coordinates and an overall isotropic U displacement factor. The only solution is to use chemically sound geometrical restraints/constraints. In our instance, 58 restraints were used, effectively reducing the number of parameters sought down to $73 - 58 = 15$. Treating our two unique molecules as rigid bodies would result in *ca* $12 + 1 = 13$ parameters being determined. Our approach is more flexible and allows for a possible puckering of the C—O rings. The 58 restraints are based on the potential energy minimization of an isolated molecule of BL at $T = 0$ K using either the semi-empirical atom–atom potentials method (PM3, UHF) or the molecular mechanics method with the *MM*+ force-field parameters provided by the molecular modeling program *HyperChem*5.1 for Windows (Hypercube Inc., 1997). The results obtained are similar in the two cases [PM3,*MM*+] and the optimized molecules have a planar C—O backbone geometry. The restraints consist of selected bond lengths and selected distances between next-neighbors.

4.2.3. Rietveld refinement. We next proceeded with the Rietveld refinement, starting from the two unique $C_4H_6O_2$ molecules found and orientated in the course of the solution process described at the beginning of §4. Optimizing the molecules only was not enough to ensure a good fit against the X-ray data. Besides adding a fifth-order/six-term Chebyschev polynomial extra contribution to the background, we found it mandatory to model with the preferred orientation and did so by using the spherical harmonics implementation of the latter in the *GSAS* suite (Von Dreele, 1997). Higher orders of spherical harmonics were introduced until no substantial benefit in terms of quality factors could be obtained. Our results are reported in Table 1. Note that the redundancy factor (= number of available unique structure factors/number of degrees of freedom) is still larger than unity (1.421) even when spherical harmonics up to the order 10 are refined. This is due to the relatively high number of geometrical restraints (58), which appreciably reduces the number of free parameters from 115 down to 57. The latter number is still somewhat smaller than the number of observed reflections (81).

Table 2
Crystal data of BL.

Crystal data	
Chemical formula	$C_4H_6O_2$
M_r	86.08
Cell setting, space group	Monoclinic, $P2_1/c$
a, b, c (Å)	10.1282 (4), 10.2303 (5), 8.3133 (4)
β (°)	93.2909 (17)
V (Å^3)	859.95 (7)
Z	8
D_x (Mg m^{-3})	1.33
Radiation type	Cu $K\alpha_1$
Temperature (K)	180
Specimen form, color	Cylindrical capillary, white
Specimen size (mm)	0.5 mm diameter
Specimen preparation cooling rate (K min^{-1})	6
Specimen preparation pressure (atm.)	1
Specimen preparation temperature (K)	Cooled down from 300 to 180
Data collection	
Diffractometer	INEL CPS 120 position-sensitive detector
Data collection method	Specimen mounting: transmission Debye–Scherrer mode; $2\theta_{min}$ = 0.30205, $2\theta_{max}$ = 114.53305, increment = 0.029
Refinement	
R factors and goodness of fit	$R_p = 0.052$, $R_{wp} = 0.069$, $R_{exp} = 0.060$, $S = 1.29$
Wavelength of incident radiation (Å)	1.54056
Excluded regions	$2\theta < 10°$; $2\theta > 40°$
Profile function	CW profile function number with 21 terms†
No of parameters	115
H-atom treatment	Refined with bond and angle restraints
Weighting scheme	LOOPARRAY
$(\Delta/\sigma)_{max}$	0.01
Preferred orientation correction	Spherical harmoic: ODF; spherical harmonic order = 10‡

Computer programs used: *GSAS* (Larson & Von Dreele, 1987). † Pseudovoigt profile coefficients as parameterized in Thompson *et al.* (1987); asymmetry correction from Finger *et al.* (1994); microstrain broadening by Stephens (1999). #1(GU) = 220.927, #2(GV) = −88.488, #3(GW) = 20.788, #4(GP) = 0.000, #5(LX) = 1.657, #6(ptec) = 0.00, #7(trns) = 0.00, #8(shft) = 0.0000, #9(sfec) = 0.00, #10,(S/L) = 0.0000, #11(H/L) = 0.0000, #12(eta) = 0.0000, #13(S400) = 0.0E = 0.00, #14(S040) = 0.0E + 00, #15(S004) = 0.0E + 00, #16(S220) = 0.0E + 00, #17(S202) = 0.0E + 00, #18(S022) = 0.0E + 00, #19(S301) = 0.0E + 00, #20(S103) = 0.0E + 00, #21(S121) = 0.0E + 00. Peak tails are ignored where the intensity is below 0.0001 times the peak. Anisotropic broadening axis: 0.0 0.0 1.0. ‡ Index = 2 0 −2, coeff = −0.1928; index = 2 0 0, coeff = 0.4183; index = 2 0 2, coeff = 0.0753; index = 4 0 −4, coeff = 0.1166; index = 4 0 −2, coeff = 1.1450; index = 4 0 0, coeff = 0.2432; index = 4 0 2, coeff = 0.6345; index = 4 0 4, coeff = 0.6219; index = 6 0 −6, coeff = −1.9053; index = 6 0 −4, coeff = 1.2835; index = 6 0 −2, coeff = −0.3569; index = 6 0 0, coeff = −2.1792; index = 6 0 2, coeff = 0.2381; index = 6 0 4, coeff = 2.4571; index = 6 0 6, coeff = 0.9538; index = 8 0 −8, coeff = 0.9905; index = 8 0 −6, coeff = −0.0950; index = 8 0 −4, coeff = 1.6723; index = 8 0 −2, coeff = −1.9020; index = 8 0 0, coeff = 3.0183; index = 8 0 2, coeff = −0.7880; index = 8 0 4, coeff = 1.3471; index = 8 0 6, coeff = −1.1220; index = 8 0 8, coeff = 1.8006; index = 10 0 −10, coeff = −0.5927; index = 10 0 −8, coeff = 1.0910; index = 10 0 −6, coeff = −0.3130; index = 10 0 −4, coeff = 1.6547; index = 10 0 −2, coeff = −1.0295; index = 10 0 0, coeff = 2.0994; index = 10 0 2, coeff = 0.2394; index = 10 0 4, coeff = −0.3914; index = 10 0 6, coeff = 0.3136; index = 10 0 8, coeff = 1.0738; index = 10 0 10, coeff = −0.8861. Preferred orientation correction range: −0.40080–3.82007.

We found that neither anisotropic linewidths nor asymmetric lineshapes were warranted by the data and did not include either effect in our final refinement, the details of which are gathered in Table 2. Fig. 1(*a*) shows the final fit between calculated and observed patterns. It corresponds to a satisfactory crystal-structure model indicator $R_{F^2} = 0.0684$,

Table 3
Selected bond lengths distances (Å) in BL_a and BL_b.

BL_a		BL_b	
C1*a*—O2*a*	1.4398 (8)	C1*b*—O2*b*	1.4399 (8)
C1*a*—C2*a*	1.5495 (7)	C1*b*—C2*b*	1.5495 (8)
C2*a*—C3*a*	1.5294 (7)	C2*b*—C3*b*	1.5294 (8)
C3*a*—C4*a*	1.5297 (6)	C3*b*—C4*b*	1.5298 (7)
C4*a*—O1*a*	1.2099 (5)	C4*b*—O1*b*	1.2099 (6)
C4*a*—O2*a*	1.3600 (5)	C4*b*—O2*b*	1.3600 (7)

Table 4
Selected coordination bond angles (°) in BL_a and BL_b.

BL_a		BL_b	
C1*a*—O2*a*—C4*a*	117.9 (3)	C1*b*—O2*b*—C4*b*	117.8 (2)
C1*a*—C2*a*—C3*a*	105.4 (1)	C1*b*—C2*b*—C3*b*	105.9 (1)
C2*a*—C3*a*—C4*a*	107.2 (2)	C2*b*—C3*b*—C4*b*	106.8 (3)
O2*a*—C1*a*—C2*a*	96.5 (1)	O2*b*—C1*b*—C2*b*	99.2 (1)
O1*a*—C4*a*—O2*a*	123.0 (3)	O1*b*—C4*b*—O2*b*	123.0 (2)
O1*a*—C4*a*—C3*a*	127.4 (1)	O1*b*—C4*b*—C3*b*	127.4 (1)
O2*a*—C4*a*—C3*a*	99.0 (3)	O2*b*—C4*b*—C3*b*	101.2 (3)

profile factors $R_p = 0.0517$ and $R_{wp} = 0.0693$, and a reduced $\chi^2 = 1.671$.

Final atomic parameters can be obtained from the supplementary material,[1] and selected interatomic distances and angles as obtained from *GSAS* are displayed in Tables 3 and 4. In the case of interatomic distances (Table 4), only the first three decimal digits are really significant. Fig. 2 represents the *ORTEP*II (Burnett & Johnson, 1996; as implemented by McArdle, 1993) molecular structure and atomic numbering of BL. A view of how BL molecules are packed in the unit cell is shown in Fig. 3.

Our CIF file incorporates a 19-point fixed-point background contribution, which will not produce a nice display when the widespread *pdCIFplot* software is used (Toby, 2003*a*). In order to circumvent this deficiency, all fitted parameters were frozen, the fixed background points mixed and our former fifth-order polynomial replaced by a nineth-order one to account for the total background. The resulting CIF has been deposited as supplementary material and is best read using the companion software *CIFEDIT* (Toby, 2003*b*) or *EnCIFer* (Allen *et al.*, 2004). Our CIF files were all fine-tuned by making use of the latter program.

5. Results and discussion

The crystallographic data of BL (BL1 polymorph) fit a monoclinic lattice and are compatible with the space group $P2_1/a$ (No. 14). The atomic numbering and the molecular structure of the two independent molecules of BL (BL_a and BL_b) are compiled in Fig. 2. The molecular packing arrangement in the unit cell is shown in Fig. 3.

A search of all the mappings of the crystal structure onto itself with the *CRYCOM* program (Dzyabchenko, 1994) did not reveal any approximate pseudosymmetry or hypersymmetry (Zorky, 1996) operations which could relate the independent molecules with each other.

From a comparison of the torsion angles of the lactone rings (Fig. 4) it can be seen that the conformations of the two independent molecules (BL_a and BL_b) are markedly different from each other as well as from that used in the structure solution, especially that of molecule *A*. Indeed, the major changes between the two independent molecules involve the twist angles about O2—C1 and C1—C2, the respective differences between which amount to 9.2 and −7.7°, respectively, which is well above the experimental error (see Fig. 4, top part). Both conformations are substantially different from the conformation of the same lactone occurring as the solvent in the crystal structure of the triazaheptane derivative butyrolactone solvate (Cobbledick & Small, 1987), where the planar fragment involves all the non-H atoms except C1 rather than C2. Note that this kind of ring puckering is predicted by molecular mechanics based on the Dreiding force field (Mayo *et al.*, 1990). Certainly, the observed conformational differences are associated with the influence of the crystal packing, which reveals quite a small stabilization of puckered ring conformations with respect to the perfectly planar shape. Actually, our *ab initio* B3LYP/6-31G calculation showed an

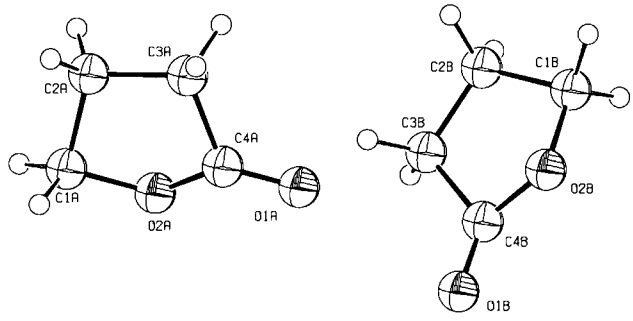

Figure 2
ORTEP (Burnett & Johnson, 1996; McArdle, 1993) drawing and atomic numbering of the molecules in the BL1 polymorph.

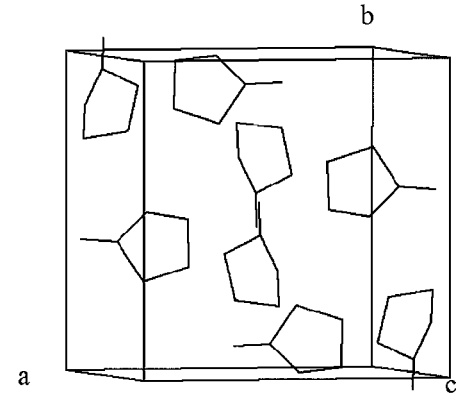

Figure 3
BL molecules packed into the BL1 unit cell (the H atoms are omitted for clarity).

[1] Supplementary data for this paper are available from the IUCr electronic archives (Reference: LC5018). Services for accessing these data are described at the back of the journal.

energy gap of $\sim 4.19\ \mathrm{kJ\ mol^{-1}}$ between an unstable planar form and a stable C2 puckered form. Such a small gap indicates that the energy basin around the ground conformational state of the molecule is quite shallow and therefore significant distortions in the other ring puckering may occur due to the weak crystal forces. One can speculate on the role of such a conformational instability in the understanding of the abnormally low freezing temperature of the present compound. Indeed, the variation in molecular shape and dimensions under thermal fluctuations may be a factor in preventing crystal ordering.

The versatility of the lactone ring conformation conveys an idea about how the physical origin of the metastable high-temperature phase can be understood. Our suggestion is that the double-cell superstructure arises due to a further increase in the number of ring conformations in the asymmetric part of the crystal as the result of populating more conformational states that fill the $4.19\ \mathrm{kJ\ mol^{-1}}$ energy gap between the ground state and the planar state. One can compare this behavior with biphenyl: this latter molecule, twisted around its axis in the gas phase, takes a perfectly planar conformation in the crystalline state at room temperature, whereas at 40 K it changes into a non-planar form again as a result of a superstructural phase transition, where a twist angle modulation takes place along the superstructure direction (Baudour & Sanquer, 1983). Energy calculations show the room-temperature phase to be a stationary point of the energy hypersurface at a small height above two equivalent minima of the modulated phase. This stationary point converts into a free-energy minimum in the room-temperature form (Dzyabchenko & Scheraga, 2004). With the present lactone, however, a similar stabilization of the planar conformation is not reached below the melting point because the energy separation between the planar and the puckered forms in the isolated molecule seems to be too high and not compensated enough by the energy of crystal packing.

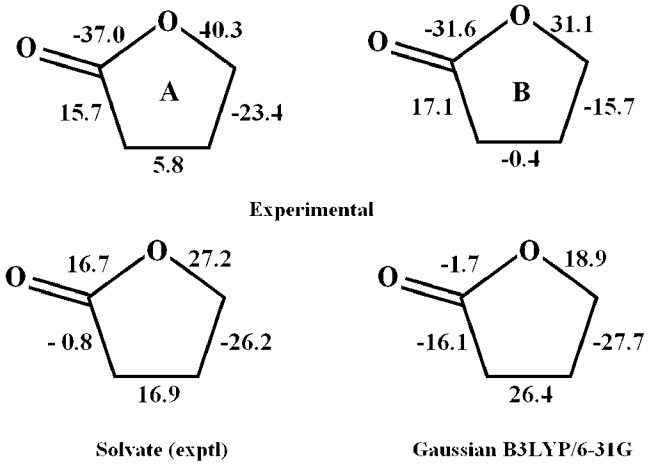

Figure 4
Comparison of torsion angles (°) in the lactone ring.

6. Conclusion

X-ray powder diffraction has been performed at 180 K on γ-butyrolactone, an organic dipolar aprotic solvent which is a popular component of electrolytes designed for lithium-ion batteries. Two polymorphs, BL1 and BL2, have been observed at T = 180 K. The first stable polymorph BL1 was solved by global energy minization and refined. Two distinct conformations of BL molecules in this solid phase are found, which differ mainly in the torsion angles. This may be explained by strong interactions between BL molecules in the solid state, as previously observed in the liquid state. The detailed structure of the second metastable polymorph BL2 (triclinic, Z = 16, eight independent molecules) is still to be determined.

References

Allen, F. H., Johnson, O., Shields, G. P., Smith, B. R. & Towler, M. (2004). *J. Appl. Cryst.* **37**, 335–338.
Allen, M. P. & Tildesley, D. J. (1987). *Computer Simulation of Liquids.* New York: Oxford University Press.
Allinger, N. L., Chen, K., Rahman, M. & Pathiaseril, A. (1991). *J. Am. Chem. Soc.* **113**, 4505–4517.
Allinger, N. L., Chen, K.-H. & Lii, J.-H. (1996). *J. Comput. Chem.* **17**, 642–668.
Allinger, N. L., Zhu, Z.-Q. S. & Chen, K. (1992). *J. Am. Chem. Soc.* **114**, 6120–6133.
Andrande, J., Böes, E. S. & Stassen, H. (2002). *J. Phys. Chem. B*, **106**, 13344–13351.
Baudour, J. L. & Sanquer, M. (1983). *Acta Cryst.* B**39**, 75–84.
Boultif, D. & Louër, D. (1991). *J. Appl. Cryst.* **24**, 987–993.
Burnett, M. N. & Johnson, C. K. (1996). *ORTEP*II. Report ORNL-6895. Oak Ridge National Laboratory, Tennessee, USA.
Chagnes, A., Allouchi, H., Carré, B., Oudou, G., Willmann, P. & Lemordant, D. (2003). *J. Appl. Electrochem.* **33**, 589–595.
Chagnes, A., Carré, B., Lemordant, D. & Willmann, P. (2001). *Electrochim. Acta*, **46**, 1783–1791.
Chagnes, A., Carré, B., Lemordant, D. & Willmann, P. (2002). *J. Power Sources*, **109**, 203–213.
Chagnes, A., Carré, B., Willmann, P., Dedryvère, R., Gonbeau, D. & Lemordant, D. (2003). *J. Electrochem. Soc.* **159**, A1255–A1261.
Chagnes, A., Mialkowski, C., Carré, B., Lemordant, D., Agafonov, V. & Willmann, P. (2001). *J. Phys. IV*, **11**, 41–45.
Chagnes, A., Nicolis, S., Carré, B., Willmann, P. & Lemordant, D. (2003). *ChemPhysChem*, **4**, 559–566.
Cobbledick, R. E. & Small, R. W. H. (1987). *Acta Cryst.* C**43**, 1341–1344.
Dauber-Osguthorpe, P., Roberts, V. A., Osguthorpe, D. J., Wolff, J., Genest, M. & Hagler, A. T. (1981). *Protein Struct. Funct. Genet.* **4**, 31–47.
Dzyabchenko, A. V. (1983). *Acta Cryst.* A**39**, 941–946.
Dzyabchenko, A. V. (1987). *J. Struct. Chem.* **28**, 862–869.
Dzyabchenko A. V. (1994). *Acta Cryst.* B**50**, 414–425.
Dzyabchenko, A. V. (2001). PMC, Version 2001. Karpov Institute of Physical Chemistry, Moscow, Russia.
Dzyabchenko, A. V. & Agafonov, V. (1995). Proc. of the 28th Annual Hawaii Intl Conference on System Sciences 1995. Biotechnology Computing, edited by L. Hunter & B. D. Shriver, Vol. 5. Los Alamitos, CA: IEEE Computer Society Press.
Dzyabchenko, A. & Scheraga, H. A. (2004). *Acta Cryst.* B**60**, 228–237.
Eijck, B. P. van (2002). *J. Comput. Chem.* **23,** 456–462.
Eijck, B. P. van & Kroon, J. (2000*a*). *Acta Cryst.* B**56**, 535–542.

Eijck, B. P. van & Kroon, J. (2000*b*). *Acta Cryst.* B**56**, 745.
Finger, L. W., Cox, D. E. & Jephcoat, A. P. (1994). *J. Appl. Cryst.* **27**, 892–900.
Frisch, M. J. *et al.* (1998). *Gaussian 98*, Revision A.7. Gaussian Inc., Pittsburgh PA.
Gasteiger, J. & Marsili, M. (1980). *Tetrahedron*, **36**, 3219–3228.
Gel'fand, I. M. & Tsetlin, M. L. (1962). *Uspekhi Matematicheskih Nauk*, **17**, 3–25.
Gel'fand, I. M., Vul, Y. B., Ginzburg, S. L. & Feodorov, Y. G. (1966). *Metod ovragov v zadachakh rentgenostructurnogo analiza.* Nauka, Moscow. 41 pp.
Hirshfeld, F. L. (1968). *Acta Cryst.* A**24**, 301–311.
Hypercube Inc. (1997). *Hyperchem Professional*, Release 5.1. Gainesville, FL 32601, USA.
Karfunkel, H. R., Wu, Z. J., Burkhard, A., Rihs, G., Sinnreich, D., Buerger, H. M. & Stanek J. (1996). *Acta Cryst.* B**52**, 555–561.
Larson, A. C. & Von Dreele, R. B. (1987). Report No. LAUR 86-748. *Program GSAS for Windows*, Version 15–04-04. Los Alamos National Laboratory, New Mexico, USA.
Lemordant, D., Chagnes, A., Caillon-Caravannier, M., Blanchard, F., Bosser, G., Carré, B. & Willmann P. (2002). *Material Chemistry in Lithium Batteries*, edited by N. Kumagai and S. Komaba, pp. 343–367. Kerala, India: Research SignPost.
Lii, J.-H. (2002). *J. Phys. Chem. A*, **106**, 8667–8679.
Louër, D. (1991). *Mater. Sci. Forum*, **79–82**, 17–26.
Louër, D. & Langford, J. I. (1988). *J. Appl. Cryst.* **21**, 430–437.
Louër, D. & Louër, M. (1972). *J. Appl.Cryst.* **5**, 271–275.
Louër, D., Louër, M., Dzyabchenko, V. A., Agafonov, V. & Ceolin, R. (1995). *Acta Cryst.* B**51**, 182–187.
Matias, P. M., Jeffrey, G. A., Wingert, L. M. & Ruble, J. R. (1989). *J. Mol. Struct. (Theochem.)* **184**, 247–260.
Mayo, S. L., Olafson, B. D. & Goddard III, W. A. (1990). *J. Phys. Chem.* **94**, 8897–8909.
McArdle, P. J. (1993). *J. Appl. Cryst.* **26**, 752.
Mialkowski, C., Chagnes, A., Carré, B., Willmann, P. & Lemordant, D. (2002). *J. Chem. Therm.* **34**, 1847–1856.
Momany, F. A., Carruthers, L. M., McGuire, R. F. & Scheraga, H. A. J. (1974). *Phys. Chem.* **78**, 1595–1620.
Pillardy, J., Arnautova, Y. A., Czaplewski, C., Gibson K. D. & Scheraga, H. A. (2001) *Proc. Natl. Acad. Sci. USA*, **98**, 12351–12356.
Rameau, J.-P., Robinet, G. & Devilliers, J. (1998). *J. Mol. Model.* **4**, 405–416.
Robinet, G., Rameau, J.-P & Devilliers, J. (2001). *J. Mol. Model.* **7**, 43–53.
Rodriguez-Carvajal, J. (2004). *Fullprof 2k*, Version 2.6. LLB, CEA/Saclay, France.
Roisnel, T. & Rodriguez-Carvajal, J. (2002). *Mater. Sci. Forum*, **378–381**, 118–123.
Rukiah, M., Lefebvre, J., Hemon, M. & Dzyabchenko, A. V. (2004). *J. Appl. Cryst.* **37**, 464–471.
Rukiah, M., Lefebvre, J., Hernandez, O., van Beek, W. & Serpelloni, M. (2004). *J. Appl. Cryst.* **37**, 766–772.
Soetens, J.-C., Millot, C., Maigret, B. & Bako, I. (2001). *J. Mol. Liquids*, **92**, 201–216.
Stephens, P. W. (1999). *J. Appl. Cryst.* **32**, 281–289.
Sun, H., Mumby, S. J., Maple, J. R. & Hagler, A. T. (1994). *J. Am. Chem. Soc.* **116**, 2978–2987.
Sun, H., Mumby, S. J., Maple, J. R. & Hagler, A. T. (1995). *J. Phys. Chem.* **99**, 5873–5882.
Thompson, P., Cox, D. E. & Hastings, J. B. (1987). *J. Appl. Cryst.* **20**, 79–83.
Toby, B. H. (2003*a*). *J. Appl. Cryst.* **36**, 1285–1287.
Toby, B. H. (2003*b*). *J. Appl. Cryst.* **36**, 1288–1289.
Von Dreele, R.B. (1997). *J. Appl. Cryst.* **30**, 517–525.
Wakihara, M. (1998). *Li-Ion Batteries*, edited by O. Yamamoto. Berlin: Wiley-VCH.
Zorky, P. M. (1996). *J. Mol. Struct.* **374**, 9–28.